AIAA AVIATION Forum
12-16 June 2023, San Diego, CA and Online
AIAA AVIATION 2023 Forum

10.2514/6.2023-4298

Modal analysis of in-duct tonal fan noise at varying shaft speed with an iterative Bayesian inverse approach

Johann Miranda-Fuentes*, Antonio Pereira†, Marc C. Jacob‡
Univ Lyon, Ecole Centrale de Lyon, CNRS, Univ Claude Bernard Lyon 1, INSA Lyon, LMFA, UMR5509, 69130, Ecully, France

Johan Thisse§
Airbus SAS, Toulouse, France

A modal analysis is carried out during the deceleration of a fan-OGV rig. The azimuthal modal content of the two first Blade Passing Frequencies is analyzed *via* an iterative Bayesian inverse approach. Interestingly the deceleration tests show as expected that the modal distribution is modified and particularly how some dominant modes are replaced by others as the shaft speed is varied. It also suggests that the geometric arrangement of the array has an influence on the modal distribution captured by the array. The method is assessed by a comparison with steady regime measurements operated on the same rig. The test data is obtained from a fan rig test database collected in the European project TurboNoiseBB.

I. Nomenclature

$\mathbf{c}$	=	vector of unknown complex coefficients
C_m	=	modal coefficient
EO	=	engine order
f	=	frequency
K	=	number of microphones
L	=	number of unknowns
m	=	azimuthal order
M	=	highest resolved azimuthal order
n	=	radial order
$\mathbf{n}$	=	vector of complex additive noise coefficients
$\hat{p}$	=	complex acoustic pressure
$\mathbf{p}$	=	vector of complex pressure coefficients
Ω	=	rotational speed
r_0	=	radial coordinate
z_0	=	axial coordinate
Δ	=	difference
$\mu_{i,j}$	=	mutual coherence between ϕ_i and ϕ_j
ϕ	=	azimuthal coordinate
$\mathbf{\Phi}$	=	azimuthal basis matrix

II. Introduction

Several mode detection techniques have been developed over the past decades for the analysis of ducted fan noise [1–8]. The majority of them have been dedicated to steady fan operating conditions, hence it is usually assumed that the measured sound field is stationary and ergodic. During fan noise testing procedures it is common that run-ups

*Post-doctoral fellow, email: johann.miranda-fuentes@ec-lyon.fr.
†Research Engineer, email: antonio.pereira@ec-lyon.fr.
‡Professor, email: marc.jacob@ec-lyon.fr.
§Turbofan noise engineer, email: johan.thisse@airbus.com

and deceleration measurements are carried along different working lines on the fan map. On the numerical side, Computational Fluid Dynamics (CFD) simulations are often employed for the analysis of aerodynamic and aeroacoustic signatures of rotor-stator interaction. However, the numerical simulations are computed on a static point. Accounting for the computational cost of the CFD, only few operating points can generally be simulated, whereas the whole range of regimes can be investigated with the deceleration measurements. In particular use can be made of the transition between cut-on to cut-off of rotor-stator interaction modes.

Recently, the Bayesian approach has been successfully applied to estimate the broadband modal content at steady operating conditions [9]. The data has been collected during a fan rig test carried out in the framework of the EU project TurbonoiseBB at the Anecom test facility. The goal of the current work is to extend this technique to the case of deceleration tests obtained during the same experimental campaign. The focus is given to the tonal components of the fan noise in particular at the blade passing frequency (BPF) and its first harmonic. The analysis of the broadband content at varying shaft speeds is a difficult task due to the very low signal-to-noise ratio. Indeed, the signals measured by wall-flush mounted probes are dominated by pressure fluctuations associated to the turbulent boundary layer. For the tonal noise, the pressure fluctuations due to the acoustic contribution are high enough to ensure a good signal-to-noise ratio. Therefore, a good estimation of the cross-spectra between array microphones might be obtained from a Short-Time Fourier Transform (STFT).

The remainder of the paper is structured as follows. Section III gives an quick overview of the in-duct mode detection problem and the Bayesian approach that is extensively described in [9–11]. Section IV describes the test bench that provided the current database. Section V discusses the results for measured and simulated data. Finally, section VI summarises the main findings discussed herein and provides perspectives of further developments.

III. Theory

A. Modal decomposition

For a cylindrical duct, the in-duct pressure field can be expressed as a weighted sum of azimuthal and radial modes by

$$\hat{p}(z,r,\phi) = \sum_{m=-\infty}^{\infty}\sum_{n=0}^{\infty}\left[A^{+}_{m,n}\mathrm{e}^{jk^{+}_{z_{m,n}}z} + A^{-}_{m,n}\mathrm{e}^{jk^{-}_{z_{m,n}}z}\right] f_{m,n}(r)\mathrm{e}^{jm\phi} \tag{1}$$

where the indexes m and n are for azimuthal and radial orders respectively. $A^{+}_{m,n}$ and $A^{-}_{m,n}$ are the coefficients of modes propagating downstream and upstream. $k^{\pm}_{z_{m,n}}$ are the axial wavenumbers in both downstream (+) and upstream ($-$) direction and $f_{m,n}(r)$ is a normalised shape factor depending on the duct's cross section and radial boundary conditions. For more details about these terms please refer to [9].

Eq. 1 can be expressed in terms of azimuthal modes only by setting

$$C_m(z_0,r_0) = \sum_{n=0}^{\infty}\left[A^{+}_{m,n}\mathrm{e}^{jk^{+}_{z_{m,n}}z} + A^{-}_{m,n}\mathrm{e}^{jk^{-}_{z_{m,n}}z}\right] f_{m,n}(r) \tag{2}$$

giving,

$$\hat{p}(z_0,r_0,\phi) = \hat{p}(\phi) = \sum_{m=-\infty}^{\infty} C_m(z_0,r_0)\mathrm{e}^{\mathrm{j}m\phi} \tag{3}$$

where $C_m(z_0,r_0)$ are the modal amplitudes of azimuthal order m.

In practice, this decomposition is associated with a circumferential array of microphones characterized by the azimuthal coordinate ϕ of the microphones. It can be expressed in a matrix-vector notation as,

$$\mathbf{p} = \mathbf{\Phi c} + \mathbf{n}, \tag{4}$$

where: $\mathbf{p} \in \mathbb{C}^K$ is a vector of complex pressure coefficients at a given angular frequency ω (obtained from a Fourier transform), $\mathbf{n} \in \mathbb{C}^K$ a vector accounting for additive noise, $\mathbf{c} \in \mathbb{C}^L$ a vector containing the *unknown* complex coefficients and $\mathbf{\Phi} \in \mathbb{C}^{K\times L}$ a matrix with elements $e^{jm\phi}$. K is the number of microphones and $L = 2M + 1$ where M is the highest resolved azimuthal order depending on the array configuration. In turbomachinery applications, it is always below the duct cut-off frequency.

Beamforming is a well-known technique to solve Eq. 4 for the modal coefficients. This technique has however a limited resolution and poor quantification results. In addition it assumes that modes are uncorrelated, which is not the case for tonal noise due to rotor-stator interaction. To overcome these limitations, the iterative Bayesian Inverse Approach (iBIA) proposed in [9] is applied in the present work. This approach is briefly described in the next section.

B. Bayesian approach

The Bayes' theorem gives an estimate of $\mathbf{c}$ given the measurements $\mathbf{p}$ by:

$$[\mathbf{c}|\mathbf{p}] = \frac{[\mathbf{p}|\mathbf{c}][\mathbf{c}]}{[\mathbf{p}]}, \tag{5}$$

where $[\mathbf{p}|\mathbf{c}]$ the probability density function (PDF) of the likelihood model, $[\mathbf{c}]$ is the PDF of the prior distribution of the unknown coefficients $\mathbf{c}$ and $[\mathbf{p}]$ is the marginal distribution of the observations. The Bayesian formalism reduces to modelling the different PDFs based on the specifics of the problem and then solving for the posterior PDF $[\mathbf{c}|\mathbf{p}]$. The approach employed here follows from previous work [9–11]. In particular the likelihood is modelled as a complex Gaussian distribution whereas the prior is modelled by a Generalized Multivariate Complex Gaussian distribution. The details of the approach and the resulting algorithm are given in [9]. In brief, it comes down to a minimization problem involving an ℓ_2-norm on the data-fitting term and an ℓ_p-norm as a penalty term. For the preliminary results presented in the next section, a value of $p = 1$ has been chosen in the minimization problem. Other values of p might be interesting for instance to highlight some aspects of tonal noise analyses, such as enforcing the sparsity of the solution if it is known *a priori* that a small number of modes are dominant.

IV. Experimental set-up

The data used herein originate from the experimental database obtained during the EU project TurboNoiseBB*, in which a large fan rig test was operated over several working lines with emphasis on approach, cutback and sideline flight conditions. A sketch of the ducted test-section is shown in Fig. 1. The fan stage consisted of a 20 blades fan and a 44 vanes stator. Besides 3 component radial hotwire measurements along several axial positions in the rotor wake, a number of microphones were distributed in the duct and the far field. The in-duct microphone arrays were located both at the intake (CMD1) and in the bypass duct (CMD3 and AX1). The axial array was composed of 60 regularly spaced microphones, whereas each azimuthal ring was composed of 100 non-uniformly distributed probes according to the array optimization technique proposed by Rademaker et al. [12]. The data retrieved from this optimized array allow for modal detections up to $m = \pm 79$ with reduced aliasing.

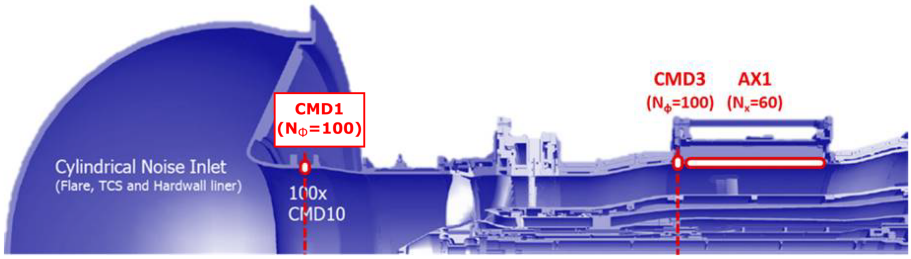

Fig. 1 Sketch of the fan rig showing the in-duct microphone arrays.

Data were acquired at a fixed sampling frequency from 100% ND to 30% ND (Nominal Drive ND = 7718 rpm) for about 9 minutes. Additionally, a tachometer trigger signal delivering one pulse per revolution was also recorded. The instantaneous rotational speed during the deceleration is shown in Fig. 2.

*https://cordis.europa.eu/project/id/690714

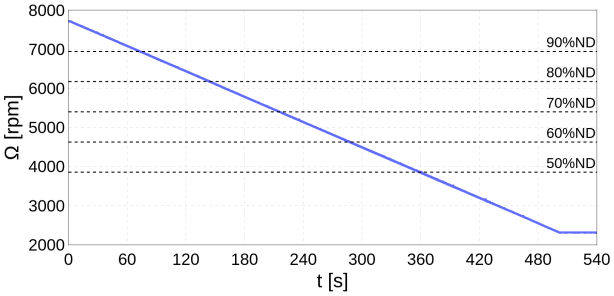

Fig. 2 Instantaneous shaft speed during the deceleration.

V. Results

A. Experimental results

Since tonal noise is related to multiples of the rotational frequency, the tachometer signal is used to resample the wall-pressure time signals from time to angular domain. Thus a fixed number of synchronized samples per rotor revolution is obtained. A Fourier transform is applied to blocks of a fixed number of revolutions, which is equivalent to a fixed engine order resolution.

A fixed engine order resolution implies a variable frequency resolution according to the following expression:

$$\Delta f = \Delta EO \frac{\Omega}{60}$$

with Ω the rotor speed in rpm. Fig. 3a shows the variation of the frequency resolution for blocks of 10, 20, 40, and 80 revolutions. These block sizes correspond to engine order resolutions of 0.1, 0.05, 0.025 and 0.0125 respectively. For the 10 revolutions block, the slope is quite high compared to that for the 40 and 20 revolutions blocks. The relative variation of the shaft speed would be helpful to choose a block size.

The relative variation of shaft speed can also be expressed as the relative variation of the Blade Passing Frequency between consecutive blocks as plotted in Fig. 3b. Negative values are expected because of deceleration but some positive values are produced by oscillations in rotational speed during deceleration. All block sizes show deviations that increase with time, and the longer the block size, the higher the deviations. As the time interval between successive rotations increases with the block size, the difference between rpm values at end and the beginning of a block also increases. However, the relative variation is rather small and remains below 1%.

The choice of 40 revolutions (engine order resolution of 0.025) is a good tradeoff between frequency resolution and shaft-speed variation within a block. Therefore, Fourier transforms have been applied to signals split into blocks of 40 revolutions.

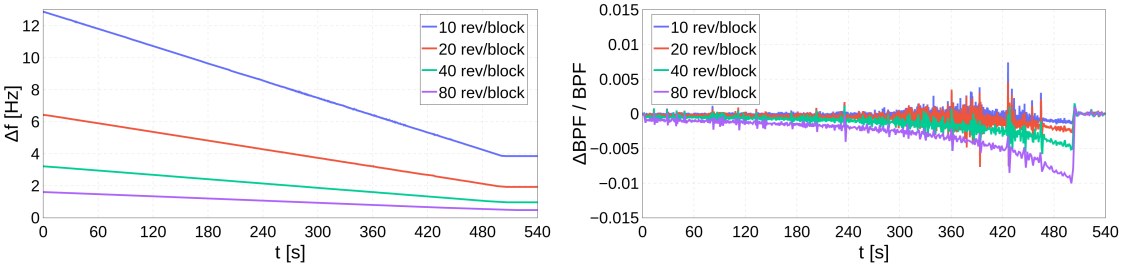

(a) Variation of frequency resolution **(b) Relative variation of Blade Passing Frequency**

Fig. 3 Impact of the number of revolutions per block on the (a) frequency resolution and (b) relative variation of shaft speed.

Results of the aft tonal noise analyzing the azimuthal ring CMD3 (see Fig. 1) are presented hereafter. Fig. 4 shows the modal spectrum computed at the first Blade Passing Frequency (BPF 1). The mode $m = 20$ dominates down to 7400 rpm approximately and then seems to scatter its energy to the $m = 19$ mode that in turn breaks down at 7200 rpm.

Modes $m = 8$ and $m = 4$ decrease fairly regularly all along the deceleration and take the lead below 7200 rpm when both $m = 20$ and 19 have dropped $15 - 20$ dB below $m = 8$ and $m = 4$. Both $m = 8$ and $m = 4$ have comparable levels down to 3700 rpm except near 70% ND, where $m = 4$ drops $5 - 10$ dB below $m = 8$ and between 60% and 50% where $m = 4$ is $10 - 20$ dB above $m = 8$. At approach flight conditions (50% ND), a switch between $m = 8$ and $m = 4$ can be seen on Fig. 4 $m = 4$ breaks down whereas $m = 8$ rises by about 20 dB in a narrow peak that is reached just below the approach point $\approx 3600 - 3800$. At lower rpm, $m = 8$ vanishes whereas $m = 4$ dominates again down to ≈ 3300. rpm. This switch between modes $m = 4$ and $m = 8$ clearly shows that the approach flight regime is at the verge between 2 modal behaviours; thus a slight over- or under- estimate can provide contradictory conclusions about which of the modes $m = 4$ or $m = 8$ dominates the BPF. It perfectly illustrates the sensitivity of the modal content with respect to slight variations of the shaft speed. Further investigation is needed to explain why and how modes that are not Tyler & Sofrin [13] modes are generated. A candidate reason for this lies in the experiment itself: indeed, as discussed in detail in [14–16] , the rotor wake measurements show evidence of blade-to-blade variations. These irregularities may give rise to any harmonic of the shaft frequency. Moreover, the additionnal modes are far below the Tyler & Sofrin modes before their cut-off. Mode $m = 20$ before cut-off is about $20 - 25$ dB above $m = 19$ and $30 - 60$ dB above $m = 4$ and $m = 8$. After the $m = 20$ cutoff, the overall level drops by $20 - 25$ dB but BPF 2 becomes dominant with respect to BPF 1 as seen on Fig. 5 with Tyler & Sofrin modes outreaching the modes $m = 4; 8; 19$ of BPF 1. Thus it is likely that some energy of BPF 1 sweeps over to BPF 2 and that the remainder of BPF 1 below 7400 rpm is essentially background noise (see e.g. [17]).

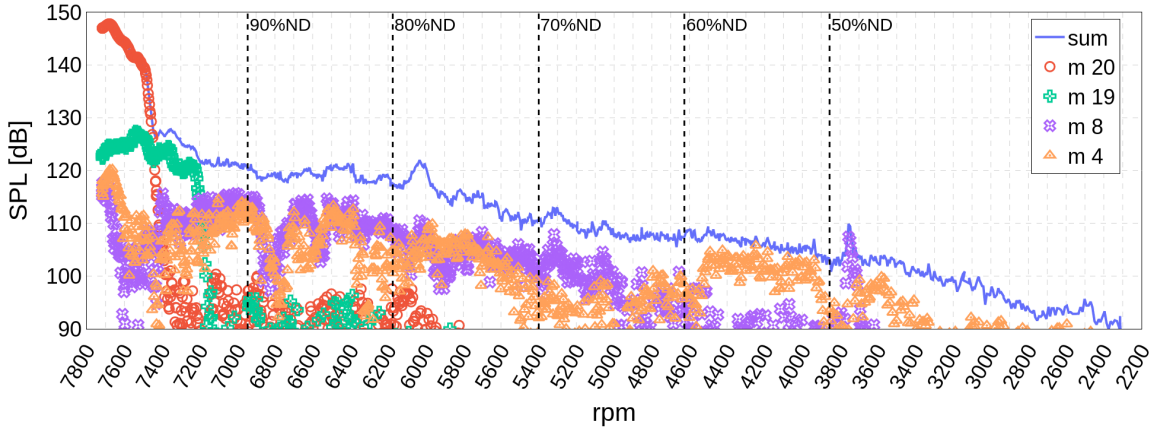

Fig. 4 Mode spectra of selected dominant modes at BPF 1 as a function of shaft speed.

A closer look to BPF 2 is provided in Fig. 5 where the modal spectrum is computed similarly as for BPF 1. The sum of modes shows an interesting pattern with peaks and troughs throughout the deceleration. The rotor alone mode $m = 40$ dominates at high shaft speed (> 7500 rpm), competes with mode $m = -4$ in between ≈ 7500 and ≈ 7300 before being cut-off around 7300 rpm. At lower shaft speeds the rotor-stator interaction mode $m = -4$ dominates the spectrum and almost matches the overall level with a few exceptions. For example, at 6400 rpm there is a significant drop with respect to the total level. The CMD3 microphones are flush mounted at the duct wall. The acoustic pressure drops observed in Fig. 5 might be due to a destructive interference (cancellation) of the pressure associated with higher radial orders n of the azimuthal mode $m = -4$. Indeed, modes associated to rotor-stator interaction are expected to be correlated for tones.

A full azimuthal and radial mode decomposition (ARMD) would be helpful to gain a better insight into modal interaction. In addition, ARMD allows to separate downstream from upstream mode contributions. The ARMD requires knowledge of additionnal data such as mean flow velocity and sound speed. Unfortunately, these data are not avalaible for deceleration but they are for steady regime at different operating points. These steady data are used for the analysis hereafter.

Another interesting trough in Fig. 5 appears around 70% ND, which correponds to a regime for which steady measurements are available. First, the mode spectrum obtained from the azimuthal only decomposition is presented in Fig. 6. The mode $m = -4$ is dominant as expected from the Tyler and Sofrin's rule [13]. This spectrum has to be compared with that obtained from the azimuthal and radial decomposition on Fig. 7a. Data from both the CMD3 and AX1 arrays are considered for the ARMD. As can be seen, an unexpected $m = 0$ is more energetic than $m = -4$.

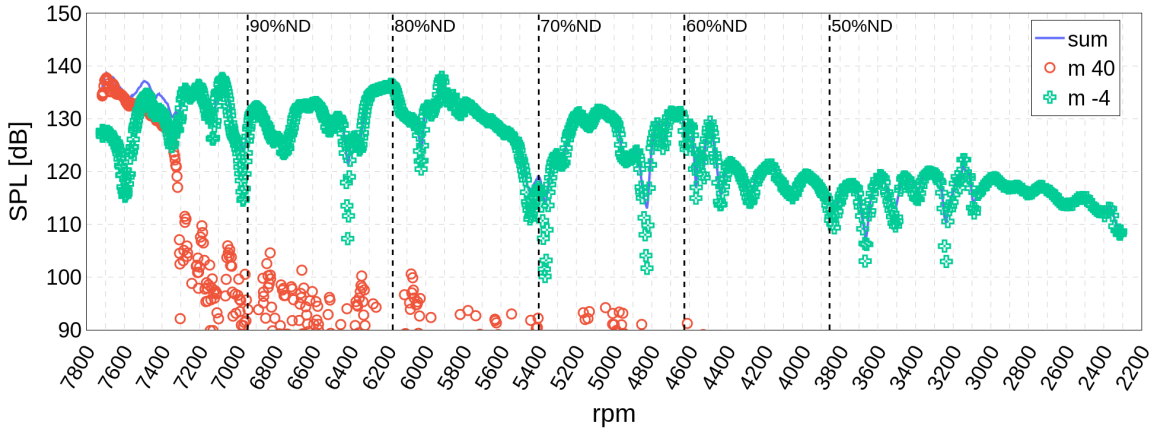

Fig. 5 Mode spectra of selected dominant modes at BPF 2 as a function of shaft speed.

Upstream, the mode spectrum in Fig. 7b shows amplitudes that are lower than the average amplitude of downstream modes and does not seem to explain the presence of the unexpected $m = 0$.

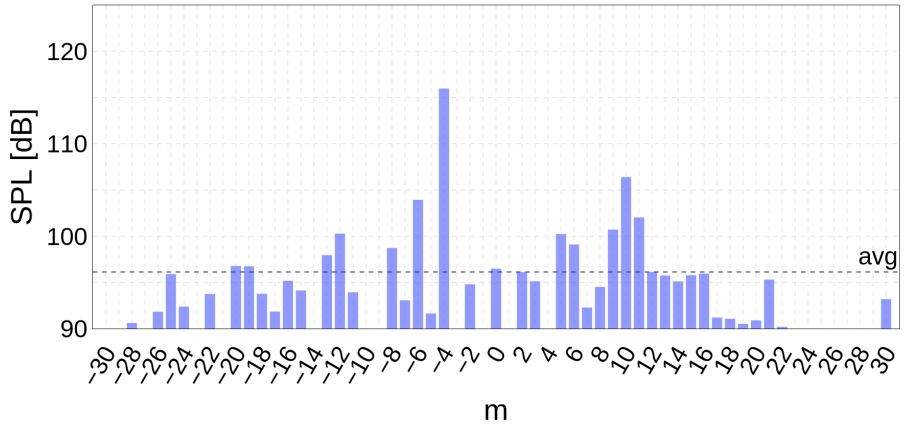

Fig. 6 Mode spectrum at BPF 2 and 70%ND (azimuthal only decomposition).

The unexpected modal content in Fig. 7a could come from the array distribution itself. The CMD3 array was optimised for mode detection up to azimuthal order $m = \pm 79$ [7, 9] with 100 sensors. This optimisation does not hold for the azimuthal and radial decomposition on both CMD3 and AX1 arrays as will be shown by the mutual coherence.

The mutual coherence given by Eq. 6 characterises the linear dependancy between columns of the modal basis $\mathbf{\Phi}$.

$$\mu_{i,j}(\mathbf{\Phi}) = \max_{i \neq j} \frac{|\boldsymbol{\phi}_i^H \boldsymbol{\phi}_j|}{||\boldsymbol{\phi}_i||_2 ||\boldsymbol{\phi}_j||_2} \tag{6}$$

The coherence matrix is symetric with unity main diagonal (self-coherence), but half of the matrix and its diagonal are set to zero for readability. The mutual coherence for the CMD3 and AX1 array is presented in Fig. 8. A diagonal line with high values and a maximum of $\mu_{(0,0),(0,1)} = 0.78$ between modes $(0, 0)$ and $(0, 1)$ can be seen in Fig. 8a. The detailed view around modes $m = -4$ and $m = 0$ in Fig. 8b shows that high values correspond to coherence between radial orders ($n = 0, 1, 2, 3$) for a fixed azimuthal order. In addition, the quite high value ($\mu_{(-4,0),(0,0)} = 0.39$) of the coherence between azimuthal orders $(-4, 0)$ and $(0, 0)$ might explain the unexepected high amplitude of $m = 0$ in Fig. 7a.

To further explore the effect of mutual coherence on the mode spectrum, simulated data is used to compare the reconstructed modal spectrum from the TurboNoiseBB array to a reference array. Since randomised arrays have been used for optimization of modal detection (see, for example, [7, 18]), the reference will be a randomised array.

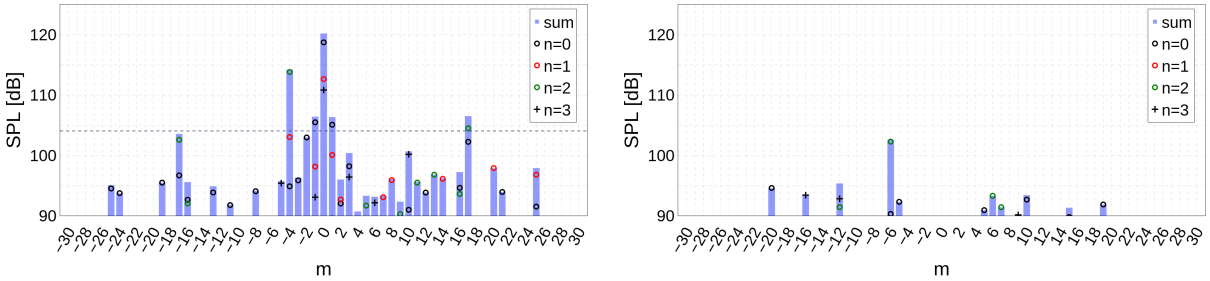

(a) ARMD (downstream) **(b) ARMD (upstream)**

Fig. 7 Modal spectra at BPF 2 and 70% ND.

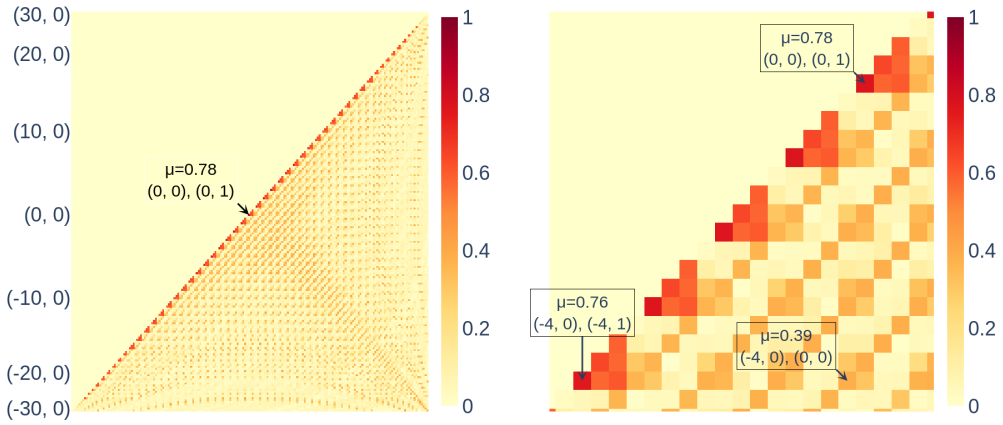

(a) Cuton modes $m = \pm 31$. **(b) Detailed view**

Fig. 8 Mutual coherence of the array consisted of both CMD3 and AX1 microphones.

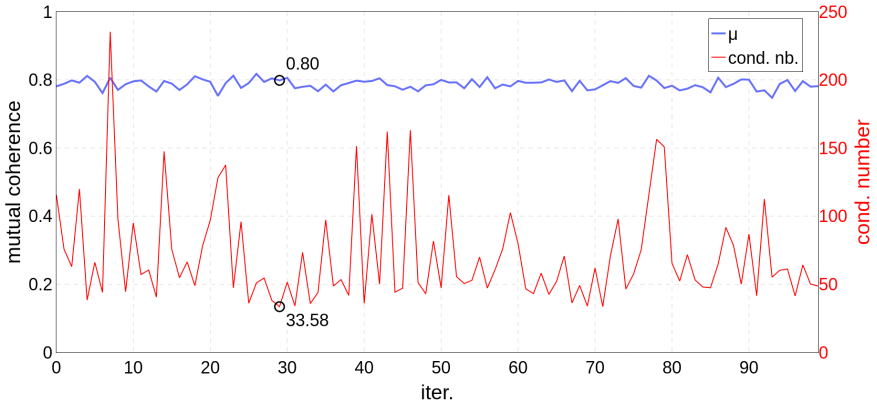

Fig. 9 Mutual coherence and condition number from random samples.

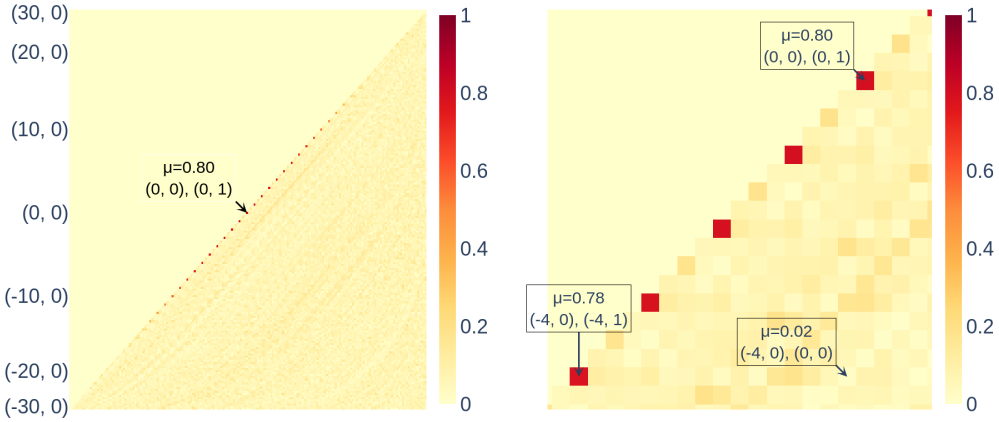

(a) Cuton modes $m = \pm 31$. **(b) Detailed view.**

Fig. 10 Mutual coherence of randomised array.

The randomised array is obtained here by extracting random samples from a large uniform array. This uniform array is constructed by setting a fixed step of 20 mm and 2° in the axial and azimuthal directions respectively. A total of 7740 coordinates are obtained for a length of 841 mm and randomised arrays are subsets of 160 out of the 7740 (CMD3 and AX1 arrays span 841 mm and total 160 sensors). The mutual coherence and condition numbers obtained for 100 trials are shown in Fig. 9. Whereas mutual coherence shows small variations, the condition number presents large deviations and peaks. Thus, the array with the minimum condition number (around trial #30 on Fig. 9) is chosen for comparison with the TurboNoiseBB array.

Compared to the TurboNoiseBB array, the randomised array still shows a maximum coherence between modes $(0, 0)$ and $(0, 1)$ but a reduced coherence between higher radial orders ($n = 2, 3$). This can be seen in Fig. 10b where peak values of the coherence are surrounded by low values. This is in contrast with the results shown in Fig. 8b, where peak values are surrounded by high values too. Moreover, the randomised array also reduces the coherence between azimuthal modes, as seen for example for the pair of modes $(-4, 0)$ and $(0, 0)$ in Fig. 10b.

B. Simulated data

The dominant modes evidenced in Fig. 7a that also show relatively high mutual coherence levels in Fig. 8, that is, the two dominant azimuthal modes $m = -4$ and $m = 0$ with their associated radial orders $n = 0, 1, 2, 3$, are chosen as input spectrum for the modal simulations. The pressure vector is constructed by adding a random noise in order to obtain a signal-to-noise ratio of SNR = 10dB. Two cases are studied, a spectrum with correlated modes, and a spectrum

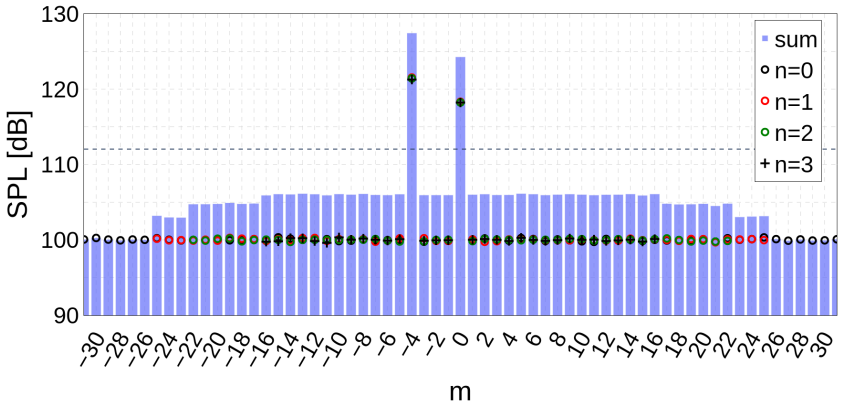

Fig. 11 Simulated input modal spectrum.

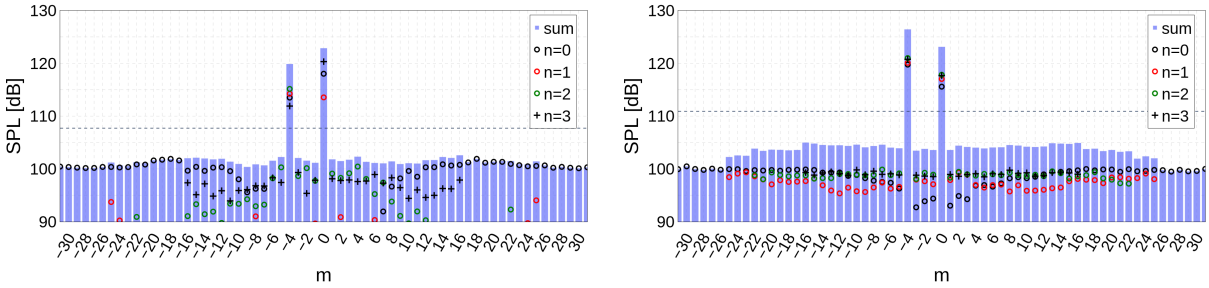

(a) TurboNoiseBB array **(b) Random array**

Fig. 12 Modal spectra obtained from simulated data.

with uncorrelated modes. For the correlated mode case, the correlation is imposed between each dominant azimuthal mode and its radial orders. For each case, the spectrum is a complex Gaussian distribution with zero mean and a case dependent covariance matrix. The simulated input data with correlated modes is shown in Fig. 11 where the average level of about 112dB is indicated by a dashed line.

The modal reconstruction obtained from simulated data with correlated modes is shown in Fig. 12. The dominant modes detected with the TurboNoiseBB array in Fig. 12a are inverted ($m = 0$ more important than $m = -4$) compared with the input spectrum in Fig. 11. In addition, the average level is about 5dB lower than the input average level. Conversely the modal detection with the randomised array yields a correct average level and dominant modes as shown in Fig. 12b. Furthermore, radial orders of dominant modes with the randomised array show small variations and are close to the input levels (about 10dB above the average level), whereas they show large variations with the TurboNoiseBB array. In particular, the mode $(m, n) = (0, 2)$ is below 90dB, that is, outside of the Figure range.

Finally, the results obtained from the simulation of uncorrelated modes are shown in Figs. 13 and 14. The Input spectrum is shown in Fig. 13 whereas the modal detection with the TurboNoiseBB array is plotted in Fig. 14a. The dominant modes and radial orders are correctly captured compared with the case of correlated input data. The average level is still about 5dB below the input data though. As can be seen in Fig. 14b, the randomised array continues to give a correct average and dominant modes levels with the randomised array.

The results from the simulated data highlight the link between the mutual coherence of array sensors and the correlation between indivdual modes. When input modes are correlated and their mutual coherence is high enough, the modal reconstruction shows an inversion of dominant modes. For the measured data, tonal noise from the rotor-stator interaction results in cross-correlated modes; therefore, the mode reconstruction should be carried out carefully high coherence values are detected by the the sensor array.

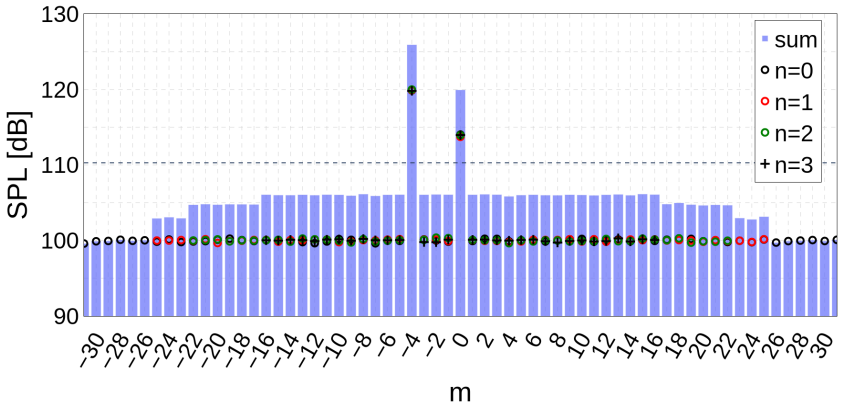

Fig. 13 Simulated input modal spectrum with uncorrelated modes.

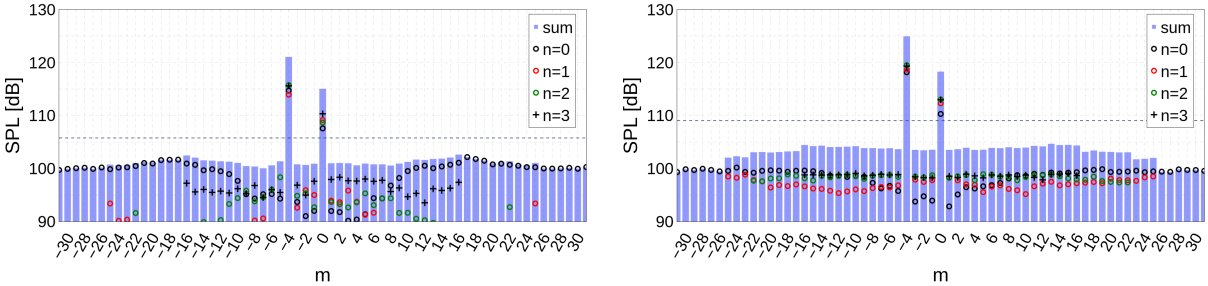

(a) TurboNoiseBB array **(b) Random array**

Fig. 14 Modal spectra obtained from simulated data with uncorrelated modes.

VI. Conclusions and outlook

Improved understanding of in-duct fan noise generation is classically obtained from azimuthal mode decompositions (AMD) or sometimes even azimuthal and radial decompositions of tonal and/or broadband noise in steady operating conditions. In the present study a novel extension to deceleration measurements is tested on the experimental database obtained during the TurboNoiseBB EU project. An iterative Bayesian Inverse Approach (iBIA) is used to solve for the modal coefficients.

The evolution of dominant modes as a function of the shaft speed highlights the rotor alone mode, rotor-stator interaction modes as well as some modes that do not correspond to Tyler & Sofrin modes. The rotor alone mode dominates the first BPF (BPF 1) at high shaft speeds but is quickly cut-off as the shaft speed becomes subsonic. At the second BPF (BPF 2), the Tyler & Sofrin rotor-stator interaction mode $m = -4$ almost matches the total pressure level throughout the deceleration showing however strong pressure level drops. A further analysis with a full azimuthal and radial mode decomposition at the 70% ND operating point shows an unexpected $m = 0$ dominant mode with high amplitude as compared to the $m = -4$ mode level. An analysis of the mutual coherence between the sensors of the array shows high coherence values between these two modes and between each of these modes and their higher radial orders. Simulated data is used to compare results from the TurboNoiseBB array against a randomised array with the same number of microphones and featuring a reduced mutual coherence level. The reconstructed mode spectrum demonstrates that correlated modes associated with high mutual coherence values, induce an amplitude inversion of the dominant modes. This conclusion is particularly important for mode detection performed at tonal frequencies since the modes generated by rotor-stator interaction are expected to be highly correlated.

Future work should address the question of how to correct the reconstructed mode amplitudes when the sensor array has high mutual coherence values.

Acknowledgments

The present work is part of the program MAMBO "Méthodes avancées pour la modélisation du bruit moteur et avion" (Advanced Methods for Engine and Aicraft Noise Modelling) coordinated by Airbus SAS. It was supported by the Direction Générale de l'Aviation Civile (DGAC) under the Grant n° 2021-50. The experimental data was obtained in the frame of the project TurboNoiseBB, which has received funding from the European Union's Horizon 2020 research and innovation program under grant agreement No. 690714. The TurboNoiseBB configuration relates to the Universal Fan Facility for Acoustics (UFFA) rig of AneCom AeroTest GmbH (Wildau, Germany)[†] equipped with the transonic ACAT1 fan.

References

[1] Joppa, P. D., "An acoustic mode measurement technique," *9th Aeroacoustics Conference*, American Institute of Aeronautics and Astronautics, 1984. https://doi.org/10.2514/6.1984-2337.

[2] Enghardt, L., Zhang, Y., and Neise, W., "Experimental verification of a radial mode analysis technique using wall-flush mounted sensors," *The Journal of the Acoustical Society of America*, Vol. 105, No. 2, 1999, pp. 1186–1186. https://doi.org/10.1121/1.425598.

[3] Castres, F. O., and Joseph, P. F., "Experimental investigation of an inversion technique for the determination of broadband duct mode amplitudes by the use of near-field sensor arrays," *The Journal of the Acoustical Society of America*, Vol. 122, No. 2, 2007, pp. 848–859.

[4] Sutliff, D. L., "Turbofan duct mode measurements using a continuously rotating microphone rake," *International Journal of Aeroacoustics*, Vol. 6, No. 2, 2007, pp. 147–170. https://doi.org/10.1260/147547207781041859.

[5] Bennett, G. J., and Fitzpatrick, J. A., "Noise-Source Identification for Ducted Fan Systems," *AIAA Journal*, Vol. 46, No. 7, 2008, pp. 1663–1674. https://doi.org/10.2514/1.33522, URL https://doi.org/10.2514/1.33522.

[6] Davis, I., and Bennett, G. J., "Novel Noise-Source-Identification Technique Combining Acoustic Modal Analysis and a Coherence-Based Noise-Source-Identification Method," *AIAA Journal*, Vol. 53, No. 10, 2015, pp. 3088–3101. https://doi.org/10.2514/1.J053907, URL https://doi.org/10.2514/1.J053907.

[7] Behn, M., Kisler, R., and Tapken, U., "Efficient azimuthal mode analysis using compressed sensing," *Proceedings of the 22nd AIAA/CEAS Aeroacoustics Conference, Lyon, France*, 2016.

[†] https://www.anecom.de/services/aerodynamic-testing/fan-noise-and-performance-test/

[8] Fauqueux, S., and Davy, R., "Modal deconvolution method in a finite circular duct, using flush-mounted microphones," *2018 AIAA/CEAS Aeroacoustics Conference*, American Institute of Aeronautics and Astronautics, 2018. https://doi.org/10.2514/6.2018-3927.

[9] Pereira, A., and Jacob, M., "Modal analysis of in-duct fan broadband noise via an iterative Bayesian inverse approach," *Journal of Sound and Vibration*, Vol. 520, 2022, p. 116633.

[10] Antoni, J., "A Bayesian approach to sound source reconstruction: Optimal basis, regularization, and focusing," *The Journal of the Acoustical Society of America*, Vol. 131, No. 4, 2012, pp. 2873–2890.

[11] Pereira, A., Antoni, J., and Leclère, Q., "Empirical Bayesian regularization of the inverse acoustic problem," *Applied Acoustics*, Vol. 97, 2015, pp. 11 – 29.

[12] Rademaker, E., Sijtsma, P., and Tester, B., *Mode detection with an optimised array in a model turbofan engine intake at varying shaft speeds*, 2001. https://doi.org/10.2514/6.2001-2181, URL https://arc.aiaa.org/doi/abs/10.2514/6.2001-2181.

[13] Tyler, J. M., and Sofrin, T. G., "Axial Flow Compressor Noise Studies," *Pre-1964 SAE Technical Papers*, SAE International, 1962. https://doi.org/https://doi.org/10.4271/620532, URL https://doi.org/10.4271/620532.

[14] Meyer, R., Hakansson, S., Hage, W., and Enghardt, L., "Instantaneous flow field measurements in the interstage section ebtween a fan and the outlet guiding vanes at different axial positions," *Proceedings of 13th European Conference on Turbomachinery Fluid Dynamics and Thermodynamics*, European Turbomachinery Soc. (Euroturbo), 2019, pp. 8–12.

[15] Lewis, D., Moreau, S., Jacob, M., and Sanjosé, M., "Fan stage broadband noise prediction using large eddy simulation and analytical models," *AIAA Journal*, Vol. 60(1), 2021, pp. 1–21.

[16] Lewis, D., de Laborderie, J., Sanjosé, M., Moreasu, S., Jacob, M., and Masson, V., "Parametric study on state-of-the-art analytical models for fan broadband interaction noise predictions," *Journal of Sound and Vibration*, Vol. 514, 2021, p. 116423.

[17] Davis, I., and Bennett, G. J., "Spectral, modal and coherence analysis of sum and difference scattering of narrowband noise in turbomachinery," *International Journal of Aeroacoustics*, Vol. 15, No. 1-2, 2016, pp. 180–206. https://doi.org/10.1177/1475472X16630860, URL https://doi.org/10.1177/1475472X16630860.

[18] Pereira, A., Salze, E., Regnard, J., Gea-Aguilera, F., and Gruber, M., *New modular fan rig for advanced aeroacoustic tests - Modal decomposition on a 20" UHBR fan stage*, ???? https://doi.org/10.2514/6.2019-2604, URL https://arc.aiaa.org/doi/abs/10.2514/6.2019-2604.